Investigation of Parameters Affecting Brain Model Validation and Brain Strains Using the SIMon Finite Element Head Model

Aaron M. Drake, Erik G. Takhounts, Vikas Hasija

Abstract Finite element (FE) models of the human brain are often validated against cadaver brain deformation experiments and are then used to predict brain injury based on strain metrics. The current study evaluates three factors hypothesized to influence FE model brain displacements: the mass of tracking targets implanted in cadaver brains, variations in brain size/shape, and variations in Neutral Density Target (NDT) locations. The first two factors were also evaluated for their effect on brain strains. Baseline simulations of five experimental impacts were conducted with the Simulated Injury Monitor (SIMon) Finite Element Head Model (FEHM). Next, independent model variations were made and the impact kinematics were again applied. Point masses were added at NDT locations, the model was scaled to various sizes/shapes, and the NDT locations were offset in three directions. Modified model results were compared to the baseline simulations. Adding point masses had almost no effect on brain displacement metrics or brain strains, while model scaling influenced both. Changing the NDT locations had the largest effect on brain displacement histories. These results indicate that size, shape and NDT location differences between experimental specimens and FE models must be accounted for in brain model validation studies.

Keywords Brain biomechanics, finite element (FE) modeling, human variability, model validation

I. INTRODUCTION

The human brain commonly experiences injury due to trauma [1] and despite extensive research efforts over the past several decades [1-35] the injury mechanisms of the brain are not entirely understood. As a material, brain tissue is nearly incompressible (high bulk modulus) and extremely soft (low shear modulus), therefore much higher loads are required to cause volume changes than shape changes [2-3]. Many researchers postulate that these changes in brain shape are the primary cause of traumatic brain injury [4-6]. A common theory is that changes in brain shape are due to shear strains that develop from rotational kinematics of the skull and brain [4][6-7].

Many studies have attempted to quantify deformations that occur in the brain due to trauma using physical models [7-10], animal surrogates [6][11-14], Post Mortem Human Subjects (PMHS) [15-18] and live human volunteers [19-21]. Of these various experimental techniques the most relevant to the present study are those conducted on PMHS's, particularly those conducted by Hardy *et al*. (2001 and 2007). These types of experiments capture the response of human head specimens subjected to levels of impact that are representative of real world car crashes and would not be ethically acceptable for live human volunteers. In these studies, human cadaver brains were implanted with radio-opaque Neutral Density Targets (NDTs) and the heads were then impacted in various directions. The displacement histories of the NDTs relative to the skull were recorded with high speed bi-planar x-ray. This type of brain displacement data is valuable in that it provides an experimental basis for the validation of computational human brain models and is directly related to brain strains.

Many FE models of the human skull and brain have been developed [22-27] and validation of these models typically consists of the following: intracranial pressures are compared with cadaver impact data from Nahum *et al.*, 1977 and relative brain displacements are compared with cadaver impact NDT data from Hardy *et al.*, 2001 and/or 2007. Despite all of the head and brain FE models in the literature displaying reasonable agreement with intracranial pressure experiments, none of the models are capable of accurately reproducing relative brain

Aaron M. Drake and Vikas Hasija are crash simulation engineers for Bowhead Logistics Solutions and are contracted by the National Highway Traffic Safety Administration (Aaron Drake Office: 202-366-6208 Email: aaron.drake.ctr@dot.gov). Erik G. Takhounts, PhD is an engineer for the Human Injury Research Division of the National Highway Traffic Safety Administration.

displacement histories of all NDTs, in all directions and for all impact cases [22-27]. For all of the models considered, the qualitative agreement in NDT displacement histories between experiment and simulation is reasonable for some cases and poor for others.

Validation of the SIMon FEHM was conducted in a previous study [22] and followed the protocol outlined above. Intracranial pressure was validated against cadaver experiments [17-18] and relative brain motion was validated against the first set of cadaver impact experiments conducted by Hardy *et al.*, 2001. More recently, relative brain motion within the SIMon FEHM was compared to the experimental results of the second set of cadaver impact experiments conducted by Hardy *et al.*, 2007 and it was found that some of the displacement signals showed reasonable agreement, while others showed poor agreement, some of which were out of phase or inverted from the experimental signals. These inconsistencies provided the impetus for the current study, which intended to determine sources of discrepancy between brain displacements measured experimentally and those calculated computationally. The influence of brain model material properties, material formulation, mesh density, boundary conditions, etc. on brain displacements has been examined previously [22][28]. Therefore, these parameters were not investigated in the present study. Instead, potential differences between experimental specimens and computational models were analyzed and their effect on relative brain displacements and strains was assessed.

Three factors were hypothesized to influence relative brain displacements and brain strains: the mass of brain tracking targets in experimental studies, the individual size and geometry of the brain and inner skull, and variability in NDT locations. To test these hypotheses, the most recent Hardy et al. (2007) NDT brain displacement study mentioned above was selected [16]. Despite the name, the neutral density targets used in the experimental study were slightly more dense than brain tissue (approximately 1.5 times as dense [16]). Therefore, the effect of these localized masses on brain deformations was examined to determine if higher density of the targets could influence experimental results. The sizes and shapes of the cadaver heads in these experiments were quite different from one another and from the 50th percentile male, providing motivation to examine the effect of brain size and shape on brain deformations. Furthermore, cadaver head (not brain) width and length dimensions are the only anthropometric measurements provided from the experimental study, so the dimensions of the brain were not known explicitly. The coordinates of the NDTs in the experimental study were provided in reference to the center of gravity (CG) of each cadaver head, which was approximated based on skull landmarks. It has been shown that head CG coordinates can vary by approximately 30 mm in X and Z directions from person to person [29]. Differences in the coordinate system origin location from experiment to computational model seem possible if not probable and may translate into discrepancies in NDT locations. Therefore, the effect of varying NDT locations was investigated to determine if errors matching the actual NDT location could influence brain displacement histories. The parameters were investigated by simulating experimental impacts computationally with an unaltered FE model, then reapplying the same impact kinematics after making specific modifications to the model and comparing the results of the original and modified models. Henceforth, the Hardy *et al*., 2007 study will be referred as *experimental* and the FE simulations of the current study will be referred to as *computational.*

II. METHODS

All of the simulations in this study were carried out using the Simulated Injury Monitor (SIMon) Finite Element Head Model (FEHM) [22]. The SIMon FEHM was developed by the National Highway Traffic Safety Administration (NHTSA) in an effort to relate three-dimensional skull kinematics to brain injury prediction metrics. The model topology and size are based on that of a 50th percentile human male. The SIMon FEHM consists of several parts: cerebrum, cerebellum, falx, tentorium, combined pia-arachnoid complex (PAC) with cerebro-spinal fluid (CSF), ventricles, brainstem, parasagittal blood vessels and the inner table of the skull (Fig. 1). The cerebrum, cerebellum and brain stem are assigned a Kelvin-Maxwell viscoelastic material definition and the

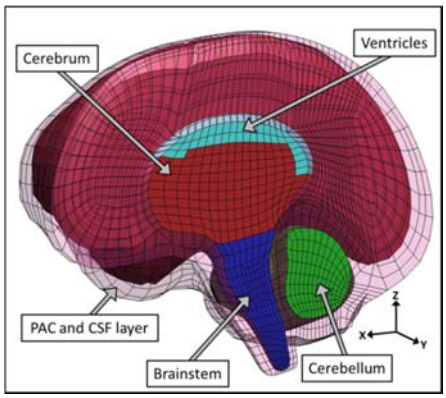

Fig. 1. Components of the SIMon FEHM.

skull is defined as a rigid shell layer. The detailed information on the development and validation of the SIMon FEHM is given in [22].

In the experimental study, the locations of NDTs within cadavers' skulls were monitored throughout impact events to quantify relative brain displacement histories. Accordingly, the displacement histories of the nodes nearest the initial NDT locations were recorded computationally in a local skull coordinate system. The SIMon FEHM nodes selected for displacement measurement will be referred to as 'NDT nodes.' Three dimensional skull kinematics were captured during the experimental cadaver head impacts using an accelerometer array package [16] and the data was acquired by plot digitization for use in the present study. The skull kinematics, specifically translational acceleration and rotational velocity histories, were applied to the rigid skull of the SIMon FEHM via prescribed motion boundary conditions. Five impact cases were simulated, consisting of impacts of three different Post Mortem Human Subjects (PMHS) at three different impact locations (Fig. 2). These five initial simulations were conducted with no modifications made to the SIMon FEHM and served as the baseline cases. Subsequently, variations were made to the SIMon FEHM or to NDT node locations, the same impact kinematics were again applied and differences between these modified cases and their respective baseline simulations were observed.

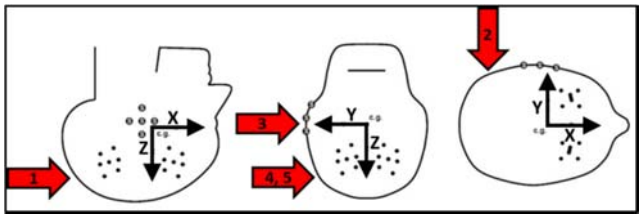

Impact Case	Cadaver #	Impact Region	Displacements Recorded
1	C288-T3	Occipital	X, Z
2	C380-T2	Parietal	X, Y
3	C380-T3	Temporal	Y, Z
4	C380-T4	Temporal	Y, Z
5	C393-T4	Temporal	Y, Z

Fig. 2. Experimental impact cases. The numbers within the arrows correspond to the impact case. The NDT cluster locations within the brain are shown on the left.

Three different factors were investigated in regards to their effect on trauma induced brain motion and strains:

1. NDT mass
2. Head size/shape
3. NDT location

In order to investigate the influence of NDT mass on deformations of the brain during trauma, point masses were added to all NDT nodes. Simulations of the five impact cases were conducted with the actual NDT mass added to the nodal mass as well as two, five, and 10 times (x2, x5, and x10) the actual NDT mass added to all NDT nodes (0.0113, 0.0226, 0.0565, 0.113 grams respectively, 20 total simulations).

Next, the effect of the size and shape of the brain and skull on brain deformations was examined. The entire SIMon FEHM was scaled positive and negative 20% in each Cartesian direction independently (±X, ±Y, ±Z), and then in all directions simultaneously (±XYZ) as illustrated in Fig. 3. Positive scaling refers to an increase in FE model size while negative scaling refers to a decrease in size. The scaling parameters selected correspond to roughly two standard deviations in head shape variability [30]. The five impact cases were simulated with each of the eight scaled configurations (40 total simulations).

Finally, the effect of NDT location on brain displacement histories was evaluated by monitoring nodal displacements at locations offset from the original NDT node. The 'new' NDT nodes were at coordinates offset from the original NDT node in the positive and negative X, Y and Z directions independently. The node nearest the offset coordinate was selected. The amount of offset was 10% of the model's overall length in each respective direction (16.6, 13.5, and 13.5 mm in X, Y, and Z, respectively as shown in Fig. 4). The six shifted NDT locations were evaluated for each of the five impact cases (30 total simulations).

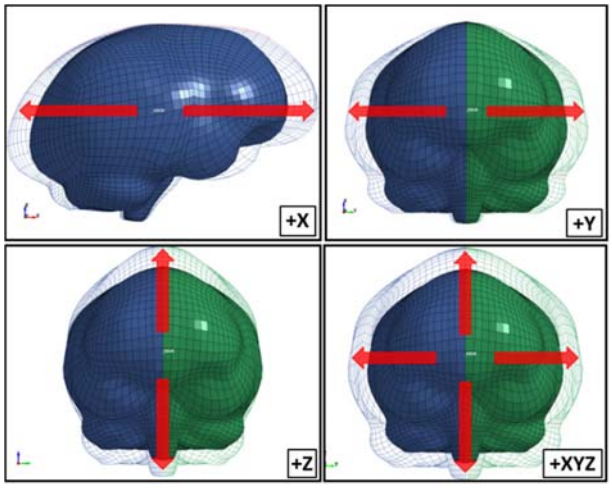

Fig. 3. Size and shape scaling of the SIMon FEHM, positive scaling shown.

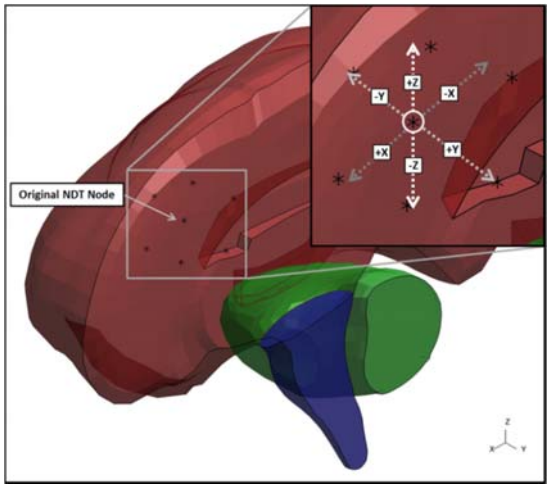

Fig. 4. NDT node location variations. Original NDT node and nodes selected at offset locations.

Measured Values

Metrics were calculated to quantify brain displacement histories and brain strains and are separated into two categories: *Displacement Metrics* and *Strain Metrics*.

Displacement Metrics: The normalized root mean squared error (NRMSE) between the experimental NDT displacement history and NDT node displacement history was calculated to quantify the 'goodness-of-fit' of the simulated results. The equation used to calculate NRMSE is:

$$\boldsymbol{NRMSE} = \left[\frac{\sum(d_{Sim}-d_{Exp})^2}{\sum d_{Exp}{}^2}\right]^{1/2}, \quad (1)$$

where d_{Sim} is the simulated displacement at a given time point and d_{Exp} is the experimental displacement at the same time point. Peak-to-peak (P2P) displacement amplitudes were calculated as the maximum minus the minimum relative NDT node displacement over the entire time history and are given in millimeters.

Strain Metrics: The maximum principal strain (MPS) to occur in any of the brain parts (cerebrum, cerebellum, and brainstem) at any time throughout the simulation was recorded. Cumulative strain damage measure (CSDM) was also calculated for all of the brain parts [31]. CSDM is the fraction of a volume that exceeds a specified strain threshold, which for the purposes of this study was set to 0.25 (i.e. CSDM(0.25)). For example, if CSDM(0.25) equals 0.05, then 5% of the brain volume reaches or surpasses a strain value of 0.25 at some point throughout the simulation.

Displacement metrics and strain metrics were calculated for the five baseline cases, the mass added cases, and the scaled cases. Only displacement metrics were evaluated for the NDT location variation cases because the global strain metrics were identical to the baseline cases (the model was unchanged, displacements were simply measured at different locations). All of the numerical results were calculated as the percent change in the measured values from the respective baseline simulation. These percent changes were then averaged over all of the impact cases in order to capture changes due to model variations. Raw averages and average magnitudes of percent changes are given for each model variation. Raw averages show whether a variation increased or decreased a measured value and average magnitudes quantify the sensitivity of a measured value to a particular variation. For model scaling and NDT location offsets the averages were also combined for the positive and negative direction for each scenario (e.g. ±X, ±Y, ±Z, ±XYZ).

In the experimental study, two clusters of seven NDTs were implanted into each cadaver brain. The displacement metrics discussed here are for the NDTs and NDT nodes at the center of each cluster (NDT 4 and NDT 11 for cluster 1 and 2, respectively [16]).

Modeling Assumptions

The simulations conducted in this study assume that rigid body kinematics of the skull are adequate to describe how impact forces are transmitted to the brain. Therefore, deformations of the skull, either local to the impact site or affecting overall skull shape, are assumed to have a negligible effect on brain deformations. The effect of NDT mass on brain deformations was examined by adding point masses at NDT node locations.

Point masses have no volume, therefore moments of inertia of the NDTs as well as initial brain strains due to the presence of the NDTs are assumed to be negligible. Furthermore, the technique used to model NDTs does not allow for any slippage of NDTs through brain material. This was considered to be inconsequential as the NDTs in the experimental study returned to their pre-impact positions [16], indicating that slippage did not occur.

III. RESULTS

For each model variation examined two sample plots are given showing the NDT displacement histories from an experimental impact, its baseline simulation and the modified simulations. These displacement plots are presented to visually highlight how the different model variations influenced NDT node motion. The sample plots are from impact case 1 (C288-T3) and impact case 4 (C380-T4) [16]. These two cases were selected to be sample plots for several reasons. First, the case 1 baseline signal shows good phase agreement but poor magnitude agreement and the case 4 baseline signal shows good magnitude agreement but is out of phase, or inverted from the experimental signal. Second, the changes in displacement histories due to model variations in these two cases are representative of the results as a whole (Appendix A shows plots of all simulated cases). Lastly, these cases highlight how significantly the parameters varied could influence the agreement with experimental results.

NDT Mass

Fig. 5 show the sample plots of the NDT node displacement histories from three mass added cases. A section of the impact case 4 plot is blown up to illustrate the effect that adding point masses at NDT nodes has on the measured displacement histories. The results from the actual NDT mass x2 simulations have been omitted because they were nearly identical to the actual NDT mass results.

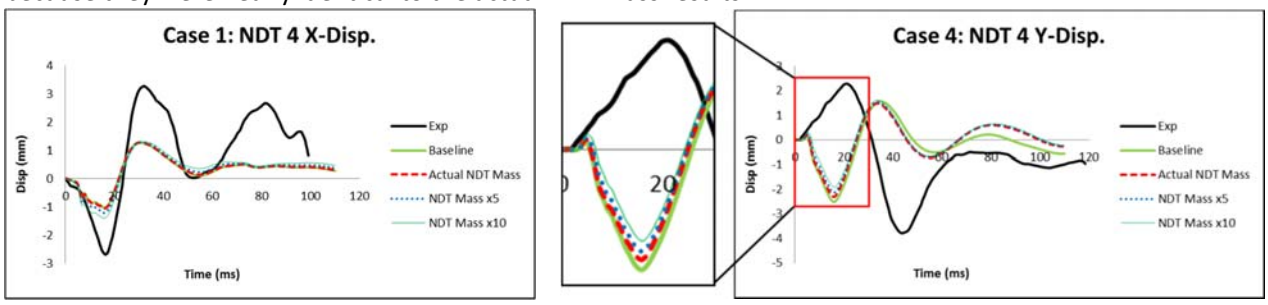

Fig. 5. NDT mass displacement histories (sample plots). Adding point masses at NDT locations had a small effect on displacement histories.

Table 1 shows the changes in NRMSE and P2P displacement for each of the NDT mass added cases. Adding point masses at the NDT locations slightly improved the fit of the simulated displacement histories with experiment (negative ΔNRMSE) and slightly increased the NDT displacement amplitudes (positive ΔP2P). The observed changes increased with increasing NDT node mass.

Table 1: NDT mass displacement metrics

ΔNRMSE in Displacement				ΔP2P Displacement			
	Actual	x5	x10		Actual	x5	x10
Raw Average	-1.40%	-2.36%	-3.46%	Raw Average	0.53%	1.88%	3.76%
Avg. Magnitude	2.33%	3.55%	5.09%	Avg. Magnitude	2.06%	4.70%	8.66%

Table 2 shows changes in MPS and CSDM associated with increasing NDT mass. All raw averages observed were positive, so increasing NDT mass increased strains in the brain. The observed changes in strain were minimal (usually <1%), but did increase slightly with increasing NDT node mass.

Table 2: NDT mass strain metrics

	ΔMPS				ΔCSDM		
	Actual	x5	x10		Actual	x5	x10
Raw Average	0.03%	0.19%	0.39%	Raw Average	0.02%	0.18%	0.22%
Avg. Magnitude	0.03%	0.19%	0.39%	Avg. Magnitude	0.16%	0.87%	1.49%

Including a point mass at the NDT locations had small effect on displacement metrics and a minimal effect on strain metrics. The changes observed did increase with increasing NDT mass; however any changes observed were small, especially for simulations conducted with the actual NDT mass added.

Head Size/Shape Variations

Fig. 6 show the sample plots with the NDT node histories for all of the scaling scenarios. Varying the size and shape of the head model slightly altered both the phase and amplitude of the displacement histories. In the case 4 example, negative scaling decreased the amplitude of the displacement and slightly improved the fit with experiment, while positive scaling had the opposite effect.

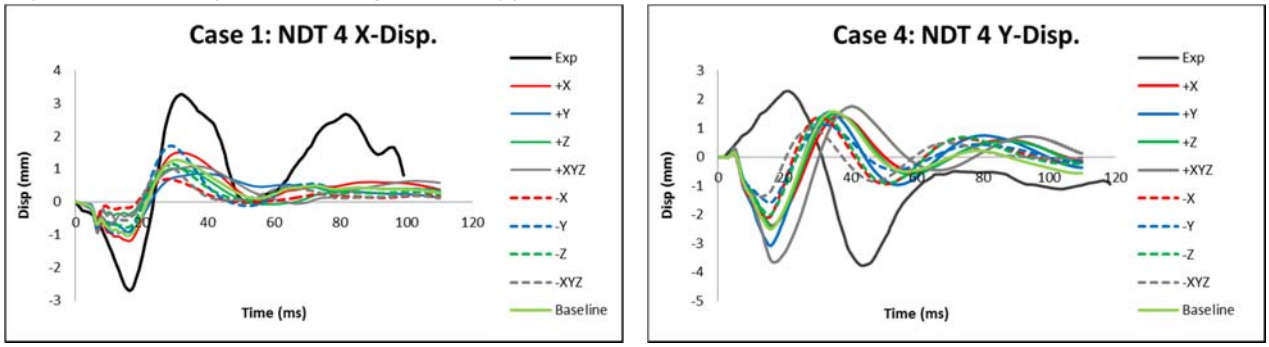

Fig. 6. Scaled model displacement histories (sample plots).

Table 3 shows changes in displacement metrics associated with each scaling scenario. Negative scaling generally improved the fit of the NDT node displacement histories with experiment, while positive scaling often degraded the fit. Positive scaling increased P2P displacements, while negative scaling decreased P2P displacements, with the exception of Y-direction scaling, which showed the opposite trend. Of the individual scaling directions, Z-direction scaling had the largest effect on measured displacement metrics.

Table 3: Head size and shape variation displacement metrics

ΔNRMSE in Displacement

	+X	+Y	+Z	+XYZ	-X	-Y	-Z	-XYZ
Raw Average	-0.83%	-0.51%	15.10%	10.26%	-3.41%	-0.72%	-4.77%	-6.50%
Avg. Magnitude	6.56%	9.75%	17.05%	15.56%	7.16%	9.34%	10.09%	13.41%

Positive and Negative Directions Combined

	±X	±Y	±Z	±XYZ
Avg. Magnitude	6.86%	9.55%	13.57%	14.49%

ΔP2P Displacement

	+X	+Y	+Z	+XYZ	-X	-Y	-Z	-XYZ
Raw Average	7.85%	-9.58%	33.61%	27.65%	-4.00%	11.89%	-11.63%	-15.09%
Avg. Magnitude	15.41%	24.93%	41.18%	32.25%	14.50%	29.12%	27.84%	22.30%

Positive and Negative Directions Combined

	±X	±Y	±Z	±XYZ
Avg. Magnitude	14.95%	27.03%	34.51%	27.27%

Table 4 shows changes in strain metrics associated with each scaling scenario. Positive scaling of the SIMon FEHM resulted in higher strains, while negative scaling decreased strains. The changes in strain metrics were most sensitive to scaling in all directions simultaneously (±XYZ), and were least sensitive to scaling in the Y-

direction (±Y). Changes in both displacement and strain metrics due to model scaling were much larger than the changes observed from adding NDT point masses.

Table 4: Head size and shape variation strain metrics

ΔMPS

	+X	+Y	+Z	+XYZ	-X	-Y	-Z	-XYZ
Raw Average	11.36%	6.96%	11.28%	19.40%	-10.01%	2.23%	-6.02%	-16.25%
Avg. Magnitude	11.36%	9.49%	11.28%	19.40%	10.01%	4.05%	6.02%	16.25%

Positive and Negative Directions Combined

	±X	±Y	±Z	±XYZ
Avg. Magnitude	10.69%	6.77%	8.65%	17.83%

ΔCSDM

	+X	+Y	+Z	+XYZ	-X	-Y	-Z	-XYZ
Raw Average	69.67%	24.91%	68.64%	160.19%	-38.91%	-3.12%	-28.20%	-68.63%
Avg. Magnitude	69.67%	27.67%	68.64%	160.19%	38.91%	12.19%	28.20%	68.63%

Positive and Negative Directions Combined

	±X	±Y	±Z	±XYZ
Avg. Magnitude	54.29%	19.93%	48.42%	114.41%

NDT Location Variations

Fig. 7 shows the sample plots with displacement histories observed at NDT locations offset from the original NDT node location in the positive and negative Z-direction (superior and inferior, respectively). Note that Z-direction offsets were 13.5 millimeters (≈½ inch). Varying the NDT location slightly had a large effect on the NDT node displacement histories. For the examples given, shifting the NDT location in the negative Z-direction (inferiorly) degraded the fit with experiment and resulted in an inverted signal for case 1. Shifting the NDT location in the positive Z-direction (superiorly) significantly improved the fit with experiment and resulted in an inverted signal for case 4.

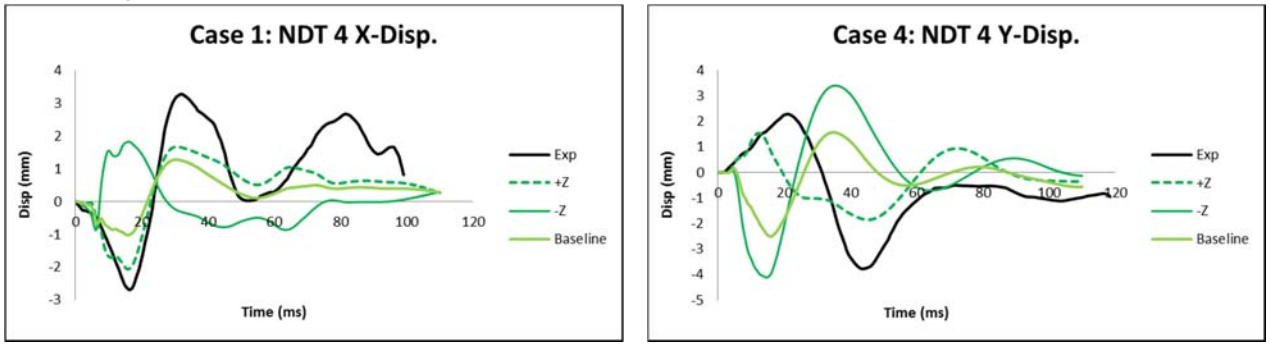

Fig. 7 Shifted NDT location displacement histories (sample plots). Only Z-direction shifts are shown. Similar results were observed for many of the Z-direction offset cases.

Table 5 shows the displacement metrics observed when the displacement histories were measured at locations offset from the original NDT node location. Both NRMSE and P2P displacement were very sensitive to changes in NDT location. The largest changes in NRMSE were observed when the location was shifted in the Z-direction.

Table 5: NDT location variation displacement metrics

ΔNRMSE in Displacement						
	+X	+Y	+Z	-X	-Y	-Z
Raw Average	9.69%	9.67%	-14.63%	-11.56%	1.84%	36.10%
Avg. Magnitude	15.64%	17.48%	18.34%	20.78%	17.91%	39.05%
Positive and Negative Directions Combined						
	±X		±Y		±Z	
Avg. Magnitude	18.21%		17.69%		28.69%	

ΔP2P Displacement						
	+X	+Y	+Z	-X	-Y	-Z
Raw Average	-0.38%	-1.84%	25.99%	-5.85%	7.36%	36.71%
Avg. Magnitude	36.21%	57.02%	41.51%	34.81%	51.20%	63.87%
Positive and Negative Directions Combined						
	±X		±Y		±Z	
Avg. Magnitude	35.51%		54.11%		52.69%	

Note that positive Z and negative X shifts resulted in large negative ΔNRMSE raw averages. Therefore, the fit with experiment was generally improved when the NDT nodes were shifted superiorly and posteriorly (see also Appendix B, Table 5).

IV. DISCUSSION

NDT Mass

This portion of the study was conducted to investigate whether the mass of targets implanted in a PMHS's brain could interfere with the displacements that those targets were intended to measure. The mass of the NDTs used in the experimental study had a negligible effect on both displacement metrics and strain metrics. However, when that mass was increased (actual NDT mass x5 and x10) the changes in measured displacement metrics increased as well. Therefore, as long as implanted targets are sufficiently small and have a density near that of brain the measured relative displacement histories are suitable for model validation.

Head Size/Shape Variations

Directional and volumetric scaling was conducted to investigate how differences in PMHS and finite element (FE) model size and shape could influence brain deformations. An example of where this would be relevant is when trying to replicate impact to a small female head with a 50th percentile male FE model (this was in fact nearly the case for the present study, as many of the anthropometric measurements of the PMHS skulls were smaller than that of a 50th percentile male). Decreasing the size of the model (negative scaling) generally improved the fit with experiment, which was expected as the model was more accurately representing the experimental specimens in these scaled configurations. Increasing the size of the model resulted in larger relative brain displacements and strains, which was also an expected result given the equal velocity equal stress scaling relationship [32-34].

The results indicate that for the same kinematic inputs the scaled models experienced different relative displacements and strains than the baseline model. This result has implications for both model validation and injury prediction. In terms of model validation, the results imply that researchers must account for differences in PMHS and FEHM size and shape when validating or tuning the properties of a model. It is suggested that the size and shape of the PMHS skull and the FEHM skull be matched as close as possible before any comparison attempts are made. This requires that several precise anthropometric measurements be provided by experimental researchers for the purpose of model validation. In terms of injury prediction, the results indicate that no single FE model will be able to accurately predict injury for all humans, even if head kinematics are precisely known. Studies have claimed to predict precise brain injuries in numerous individuals without accounting for head geometry variations [35]. The present study indicates that variations in head geometry

modulate brain strains, which are the cause of injury; therefore, studies that have not accounted for head size/shape may be misleading.

NDT Location Variations

Displacement histories were measured at nodes offset from the original NDT node locations to investigate how sensitive the displacement histories were to spatial measurement variations. This portion of the study was conducted because NDT locations in the experimental study were referenced to each specimen's approximate head center of gravity (CG), a reference point that can vary from specimen to specimen and from experiment to simulation. The results of this section indicate that relatively small NDT location changes (≈13.5 mm) can dramatically alter the simulated displacement histories and their agreement with experiment. Therefore, the differences between experimental and computational displacement histories may be largely attributed to errors matching experimental and computational NDT locations.

The changes in displacement history phase and magnitude observed at shifted NDT locations are due to the wavelike nature of deformations in the brain. The concept can be visualized by considering oscillation of a string at its second harmonic frequency (Fig. 8). Measuring displacement histories at various locations along the length of the string would result in large changes in displacement magnitude (a to b) and/or inversion of phase (a to c), as was often seen with superior shifts in NDT location in the current study. Deformation waves of the brain are three dimensional and the geometry of the medium is much more complex, but the concept is the same.

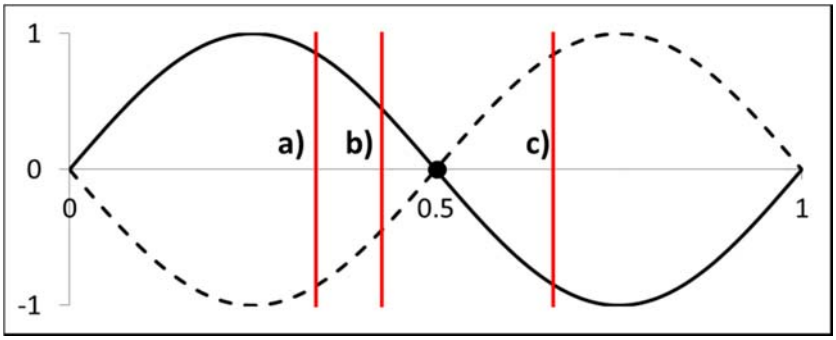

Fig. 8. String oscillating at its second harmonic frequency as an analogy for brain deformation wave motion.

No head measurement was provided from the experimental study in the Z-direction and for nearly every displacement history observed shifting the NDT location superiorly (+Z) improved the fit, while inferior shifts (-Z) almost always degraded the fit with experiment (see Appendix). This may imply that the experimental coordinate system origin was located superior to the computational coordinate system origin. Future experimental and computational efforts should aim to reduce coordinate systems discrepancies. This could be accomplished by referencing the NDT locations to multiple skull landmarks or by including CT scan images with the coordinate system and origin clearly defined.

The importance of anthropometric measurements and references in the Z-direction should be emphasized, as model scaling and NDT location offsets in the Z-direction caused large changes in displacement histories and measurements in this direction are not always provided in the literature.

Limitations

One of the major limitations of this study was that very few data points were collected for each parameter investigated. It may be useful, for example, to examine varying degrees of scaling and NDT location variations (i.e. 5, 10, 15%), in addition to the values selected for this study. Another limitation is that only one FE model was used for the simulations in this study. It is possible that FE models other than the SIMon FEHM would display different degrees of sensitivity to the variations made in this study.

V. CONCLUSIONS

The effects of three parameters on relative brain displacements and brain strains were investigated by simulating cadaver head impacts with the SIMon FEHM. The parameters considered were the mass of NDTs, the size and shape of the head model and the location of the NDTs. The mass of NDTs implanted in the brain during cadaver head impact experiments does not affect measured displacements if the targets are sufficiently small and light, as they were in the referenced experimental study. Strains induced by NDTs are negligible. Both the size and shape of the skull and brain affect relative brain displacements and strains. Increasing the size of the brain generally increases brain displacements and strains. Variations in NDT locations significantly alter the measured brain displacement histories and can substantially improve or degrade the fit with experiment.

VI. REFERENCES

[1] M. Faul, L. Xu, M. M. Wald, and V. G. Coronado, "Traumatic brain injury in the United States: emergency department visits, hospitalizations and deaths 2002–2006," *Atlanta Centers Dis. Control Prev. Natl. Cent. Inj. Prev. Control*, 2010.

[2] M. S. Estes and J. H. McElhaney, "Response of brain tissue of compressive loading," in *4th ASME Biomechanics*, 1970.

[3] K. B. Arbogast, D. F. Meaney, and L. E. Thibault, "Biomechanical Characterization of the Constitutive Relationship for the Brainstem," *39th Stapp Car Crash Conf. Proc.*, no. 13, pp. 153–159, 1995.

[4] E. G. Takhounts, "A Modern Perspective on Historical Brain Injury Research," in *IRCOBI Keynote presentation*, 2015.

[5] A. C. Bain and D. F. Meaney, "Tissue-level thresholds for axonal damage in an experimental model of central nervous system white matter injury.," *J. Biomech. Eng.*, vol. 122, no. 6, pp. 615–622, 2000.

[6] T. A. Gennarelli, L. E. Thibault, and A. K. Ommaya, "Pathophysiologic Responses to Rotational and Translational Accelerations of the Head," *SAE Tech. Pap. Ser.*, vol. 720970, pp. 296–308, 1972.

[7] A. H. S. Holbourn, "Mechanics of head injuries," *Lancet*, vol. 242, no. 6267, pp. 438–441, 1943.

[8] S. S. Margulies, L. E. Thibault, and T. A. Gennarelli, "Physical model simulations of brain injury in the primate.," *J. Biomech.*, vol. 23, no. 8, pp. 823–36, 1990.

[9] D. F. Meaney *et al.*, "Biomechanical analysis of experimental diffuse axonal injury," *J. Neurotrauma*, vol. 12, no. 4, pp. 689–694, 1995.

[10] L. Thibault, S. Margulies, and T. Gennarelli, "The temporal and spatial deformation response of a brain model in inertial loading," *SAE Tech. Pap. 872200*, 1987.

[11] T. A. Gennarelli, L. E. Thibault, J. H. Adams, D. I. Graham, C. J. Thompson, and R. P. Marcincin, "Diffuse axonal injury and traumatic coma in the primate," *Ann. Neurol.*, vol. 12, no. 6, pp. 564–574, 1982.

[12] T. Gennarelli, L. Thibault, G. Tomei, R. Wiser, D. I. Graham, and J. H. Adams, "Directional dependence of axonal brain injury due to centroidal and non-centroidal acceleration," *SAE Tech. Pap. Ser.*, vol. 872197, pp. 49–53, 1987.

[13] T. A. Gennarelli, J. M. Abel, H. Adams, and D. Graham, "Differential Tolerance of Frontal and Temporal Lobes to Contusion Induced by Angular Acceleration," *Soc. Automot. Eng. Inc.*, pp. 563–586, 1979.

[14] R. H. Pudenz and C. H. Shelden, "The Lucite Calvarium—A Method for Direct Observation of the Brain," *J. Neurosurg.*, vol. 3, no. 6, pp. 487–505, 1946.

[15] W. N. Hardy, C. D. Foster, M. J. Mason, K. H. Yang, A. I. King, and S. Tashman, "Investigation of head injury mechanisms using neutral density technology and high-speed biplanar x-ray," *Stapp Car Crash J*, vol. 45, pp. 337–368, 2001.

[16] W. N. Hardy *et al.*, "A Study of the Response of the Human Cadaver Head to Impact," *Stapp Car Crash J.*, vol. 51, no. October, pp. 17–80, 2007.

[17] A. M. Nahum, R. Smith, and C. Ward, "Intracranial Pressure Dynamics During Head Impact," *21st Stapp Car Crash Conf.*, pp. 337–366, 1977.

[18] X. Trosseille, C. Tarriere, F. Lavaste, and F. Guillon, "Development of a F.E.M. of the Human Head According to a Specific Test Protocol," *SAE Tech. Pap. 922527*, 1992.

[19] P. Bayly, T. Cohen, E. Leister, D. Ajo, E. Leuthardt, and G. Genin, "Deformation of the Human Brain Induced by Mild Acceleration," *J Neurotrauma*, vol. 22, no. 8, pp. 845–856, 2008.

[20] A. K. Knutsen *et al.*, "Improved measurement of brain deformation during mild head acceleration using a novel tagged MRI sequence," *J. Biomech.*, vol. 47, no. 14, pp. 3475–3481, 2014.

[21] A. A. Sabet, E. Christoforou, B. Zatlin, G. M. Genin, and P. V. Bayly, "Deformation of the human brain induced by mild angular head acceleration," *J. Biomech.*, vol. 41, no. 2, pp. 307–315, 2008.
[22] E. G. Takhounts *et al.*, "Investigation of traumatic brain injuries using the next generation of simulated injury monitor (SIMon) finite element head model," *Stapp Car Crash J.*, vol. 52, pp. 1–31, 2008.
[23] D. Sahoo, C. Deck, and R. Willinger, "Development and validation of an advanced anisotropic visco-hyperelastic human brain FE model," *J. Mech. Behav. Biomed. Mater.*, vol. 33, pp. 24–42, 2014.
[24] L. Zhang *et al.*, "Recent advances in brain injury research: a new human head model development and validation.," *Stapp Car Crash J.*, vol. 45, no. DECEMBER, pp. 369–394, 2001.
[25] M. Iwamoto, Y. Nakahira, and H. Kimpara, "Development and Validation of the Total HUman Model for Safety (THUMS) Toward Further Understanding of Occupant Injury Mechanisms in Precrash and During Crash," *Traffic Inj. Prev.*, vol. 16, no. sup1, pp. S36–S48, Jun. 2015.
[26] B. Yang, K. M. Tse, N. Chen, L. B. Tan, Q. Zheng, and H. M. Yang, "Development of a Finite Element Head Model for the Study of Impact Head Injury," *Biomed Res. Int.*, vol. 408278, 2014.
[27] H. Mao, L. Zhang, B. Jiang, and E. Al., "Development of a Finite Element Human Head Model Partially Validated With Thirty Five Experimental Cases," *J. Biomech. Eng.*, vol. 135, no. 11, 2013.
[28] S. Kleiven and W. N. Hardy, "Correlation of an FE Model of the Human Head with Local Brain Motion--Consequences for Injury Prediction.," *Stapp Car Crash J.*, vol. 46, no. November, pp. 123–44, 2002.
[29] J. A. Plaga, C. Albery, M. Boehmer, C. Goodyear, and G. Thomas, "Design and Development of Anthropometrically Correct Head Forms for Joint Strike Fighter Ejection Seat Testing," Wright-Patterson AFB, OH, 2005.
[30] J. Lee, S. Hwang Shin, and C. L. Istook, "Analysis of Human Head Shapes in the United States," *Int. J. Hum. Ecol.*, vol. 7, no. 1, pp. 77–83, 2006.
[31] F. A. Bandak and R. H. Eppinger, "A three-dimensional finite element analysis of the human brain under combined rotational and translational accelerations," *Stapp Car Crash Conf. STAPP 1994*, 1994.
[32] A. K. Ommaya, P. Yarnell, and A. E. Hirsh, "Scaling of Experimental Data on Cerebral Concussion in Subhuman Primates to Concussion Threshold for Man," in *11th Stapp Car Crash Conference*, 1967, pp. 73–80.
[33] R. Eppinger, E. Sun, and F. Bandak, "Development of improved injury criteria for the assessment of advanced automotive restraint systems–II," *… Highw. Traffic Saf. …*, no. September, p. 1997, 1999.
[34] R. L. Stalnaker, V. L. Roberts, and J. H. Mcelhaney, "Side Impact Tolerance to Blunt Trauma," *SAE Pap. 730979*, 2012.
[35] D. Sahoo, C. Deck, and R. Willinger, "Axonal strain as brain injury predictor based on real-world head trauma simulations.," in *IRCOBI Conference*, 2015, pp. 186–197.

VII. APPENDIX

Appendix A: Displacement Histories

NDT Mass

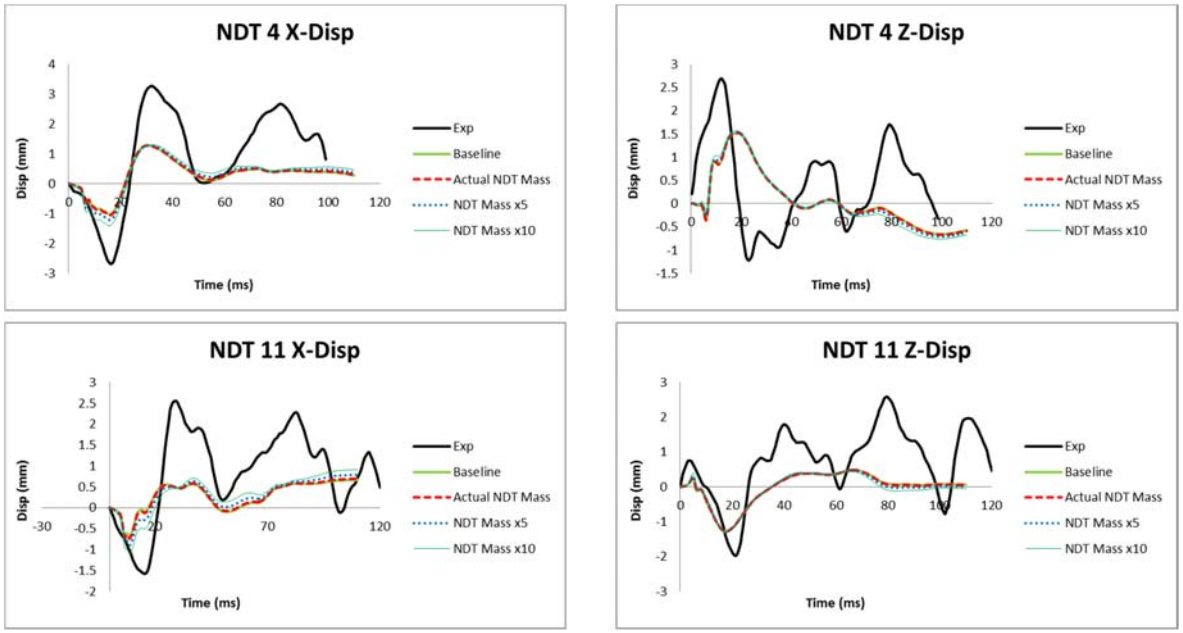

Figs. 1-4: C288-T3 NDT mass added displacement histories. NDT 4 was at the center of Cluster 1 and NDT 11 was at the center of Cluster 2.

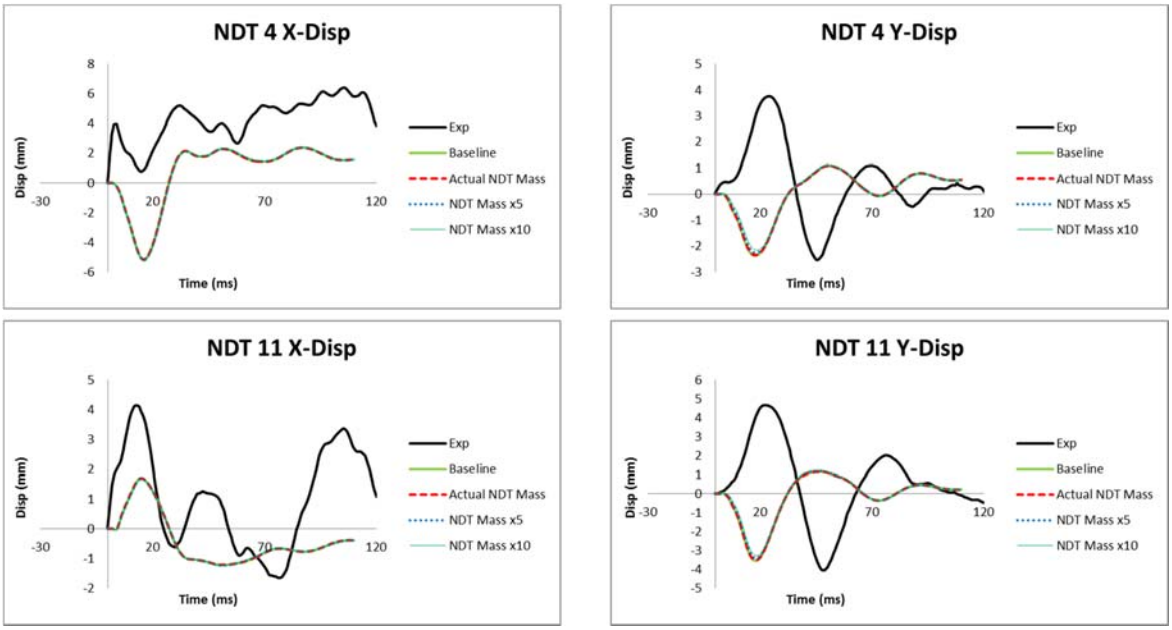

Figs. 5-8: C380-T2 NDT mass added displacement histories.

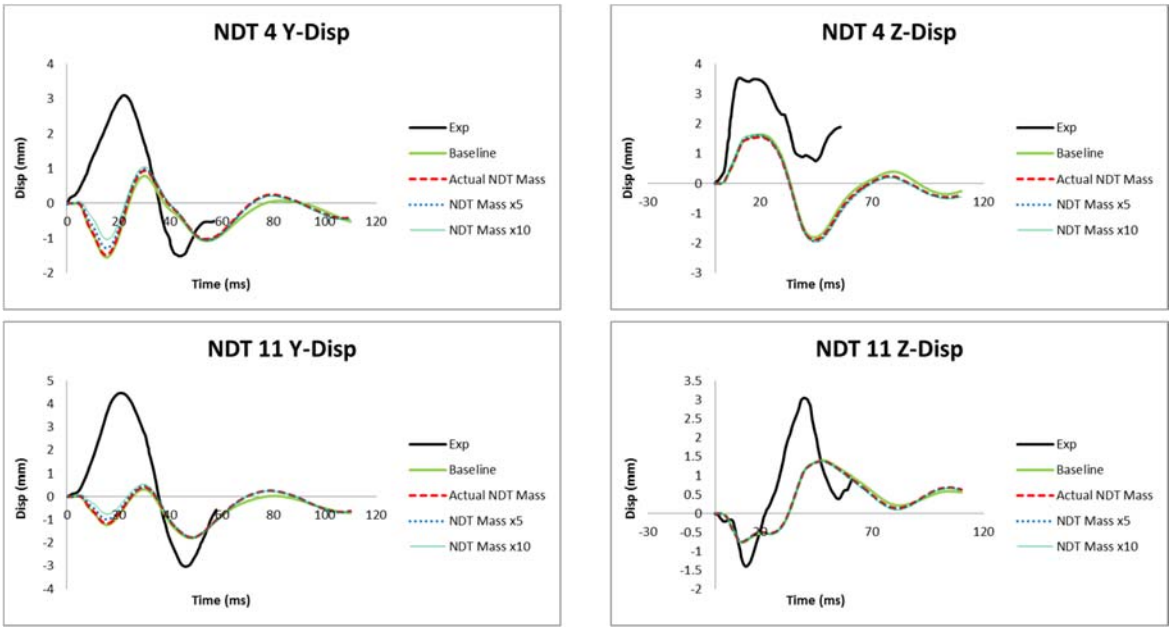

Figs. 9-12: C380-T3 NDT mass added displacement histories.

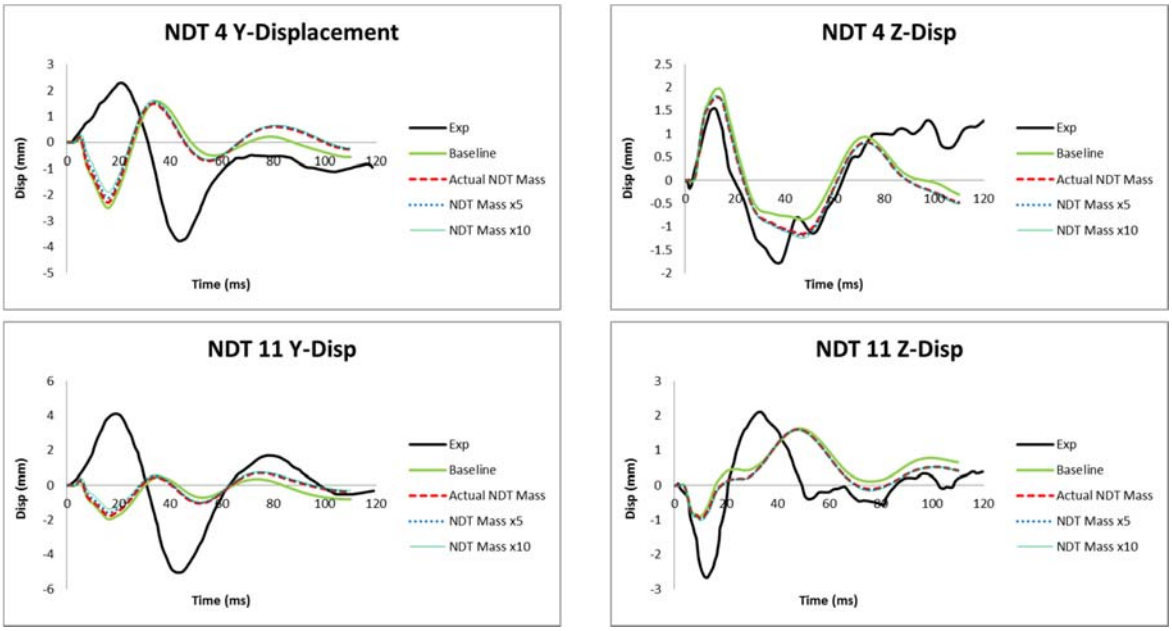

Figs. 13-16: C380-T4 NDT mass added displacement histories.

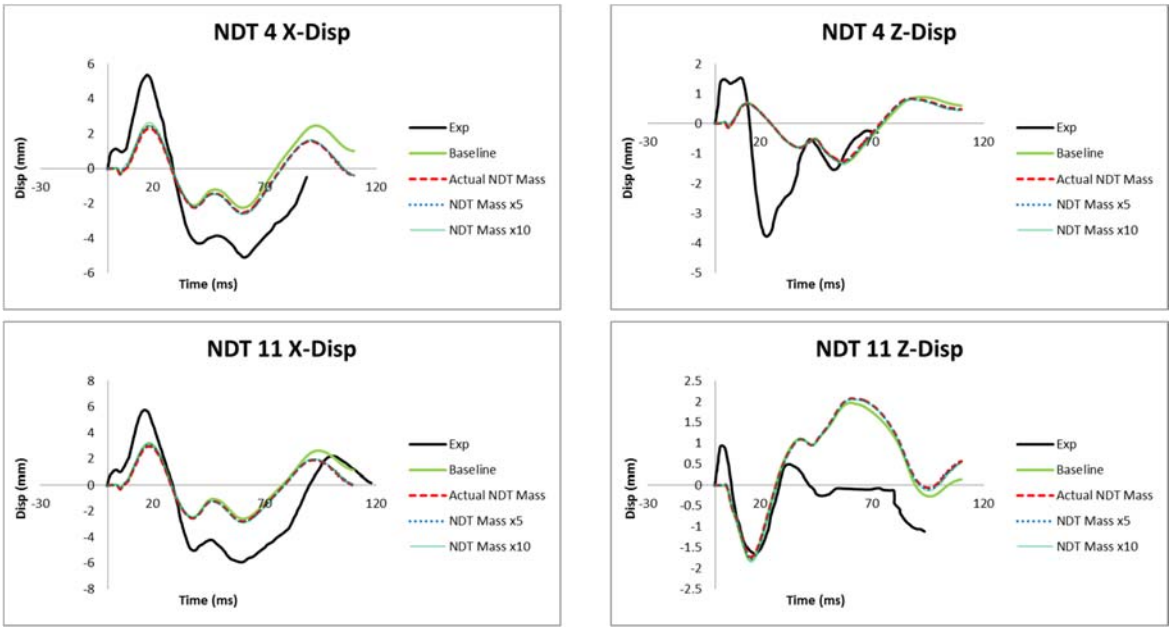

Figs. 17-20: C393-T4 NDT mass added displacement histories.

Head Size/Shape Variations

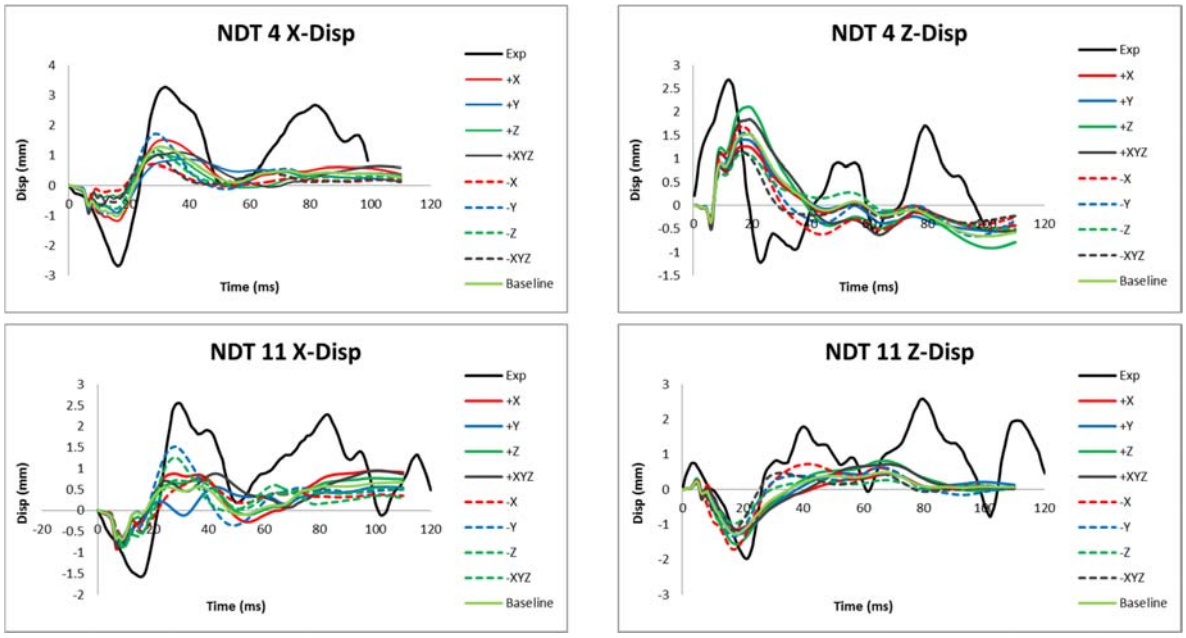

Figs. 21-24: C288-T3 NDT scaled model displacement histories.

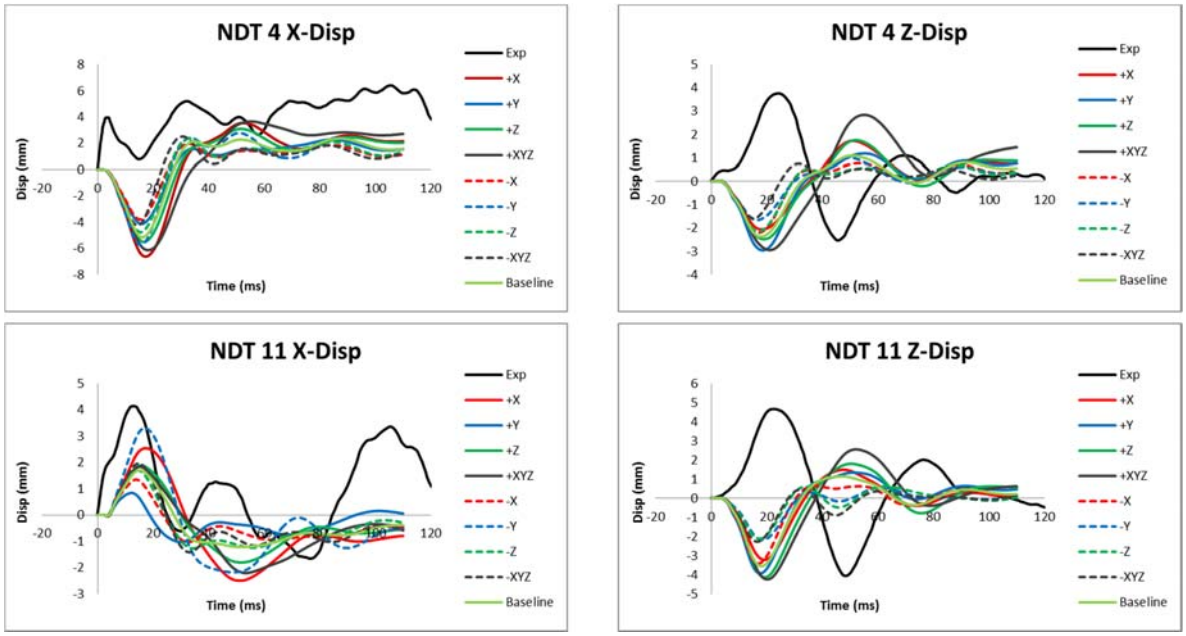

Figs. 25-28: C380-T2 NDT scaled model displacement histories.

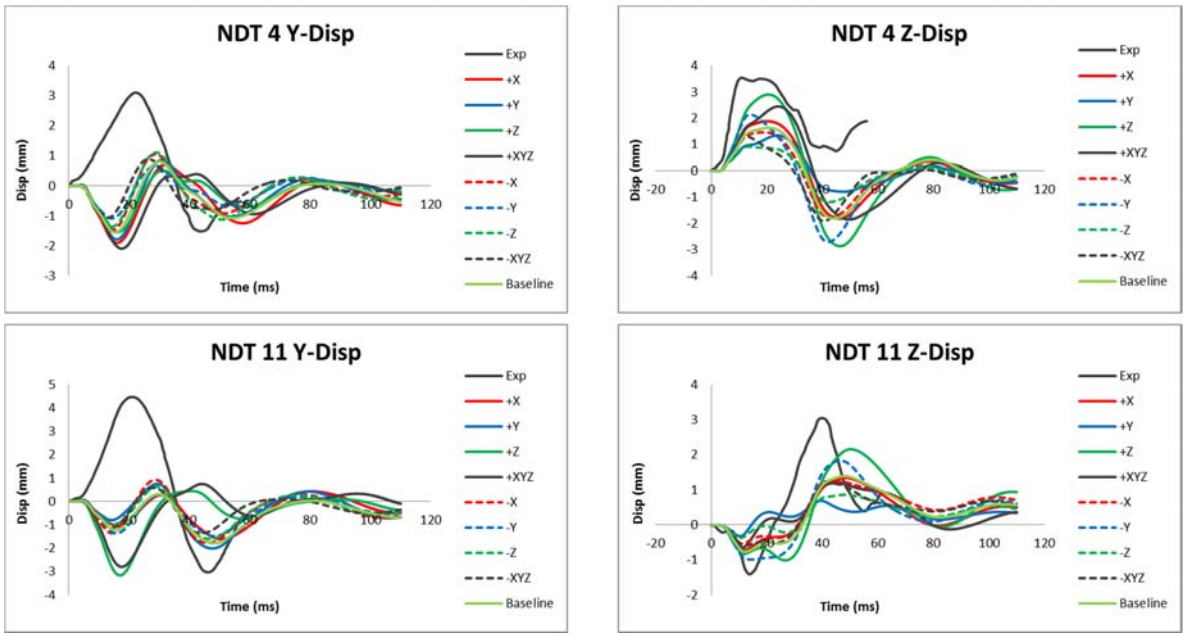

Figs. 29-32: C380-T3 NDT scaled model displacement histories.

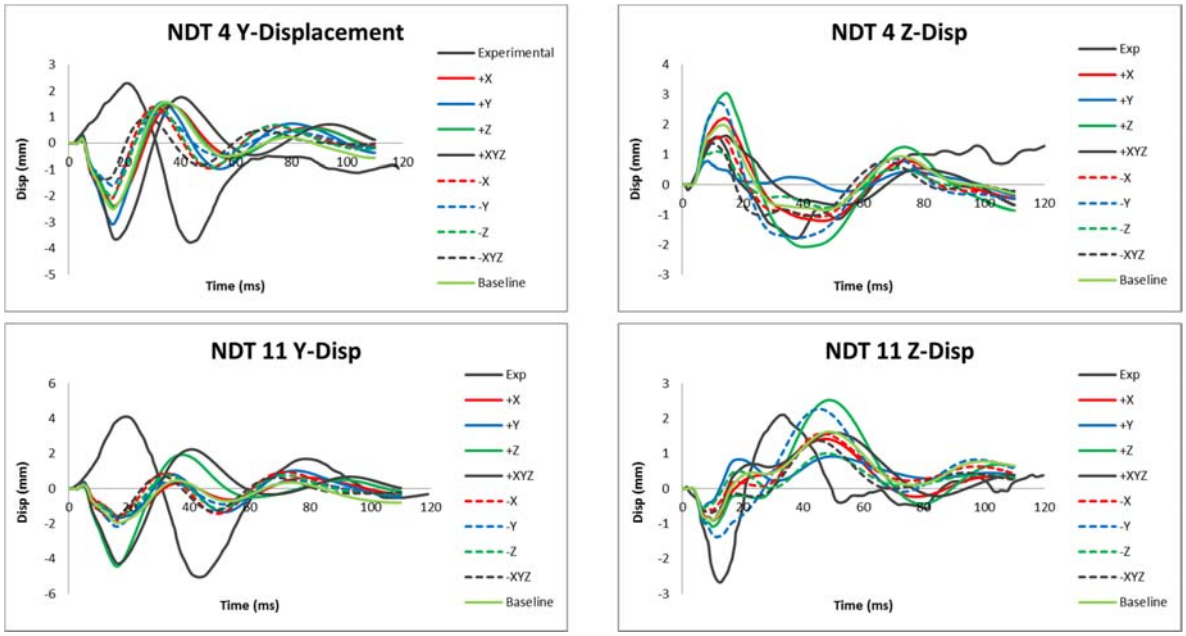

Figs. 33-36: C380-T4 NDT scaled model displacement histories.

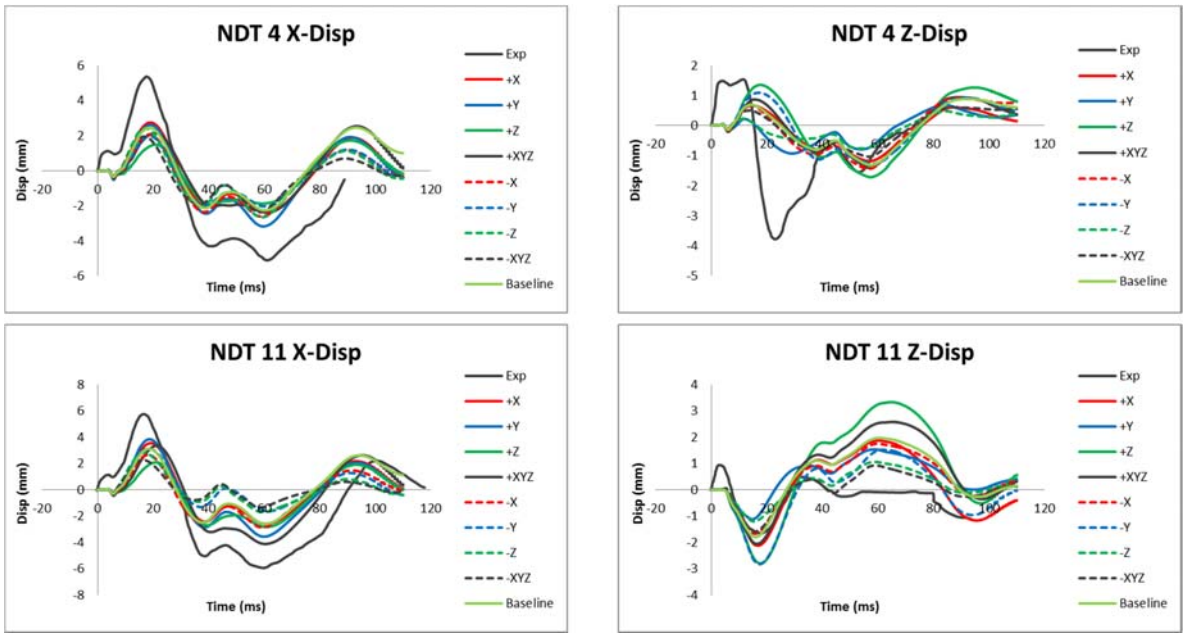

Figs. 37-40: C393-T4 NDT scaled model displacement histories.

NDT Location Variations

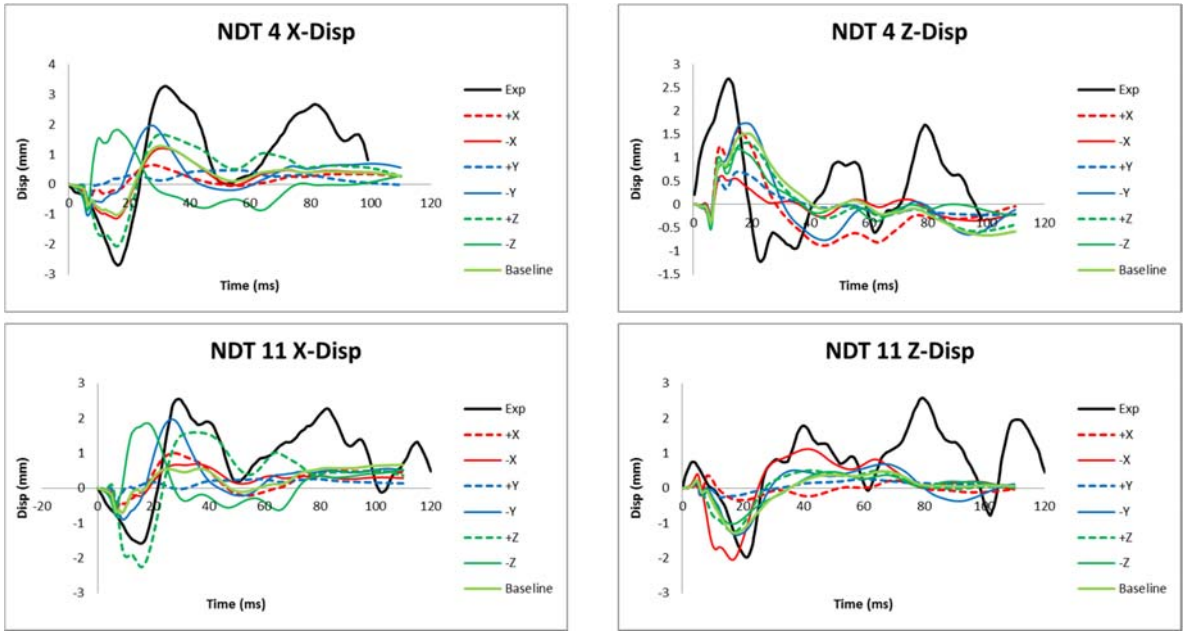

Figs. 41-44: C288-T3 NDT offset NDT location displacement histories.

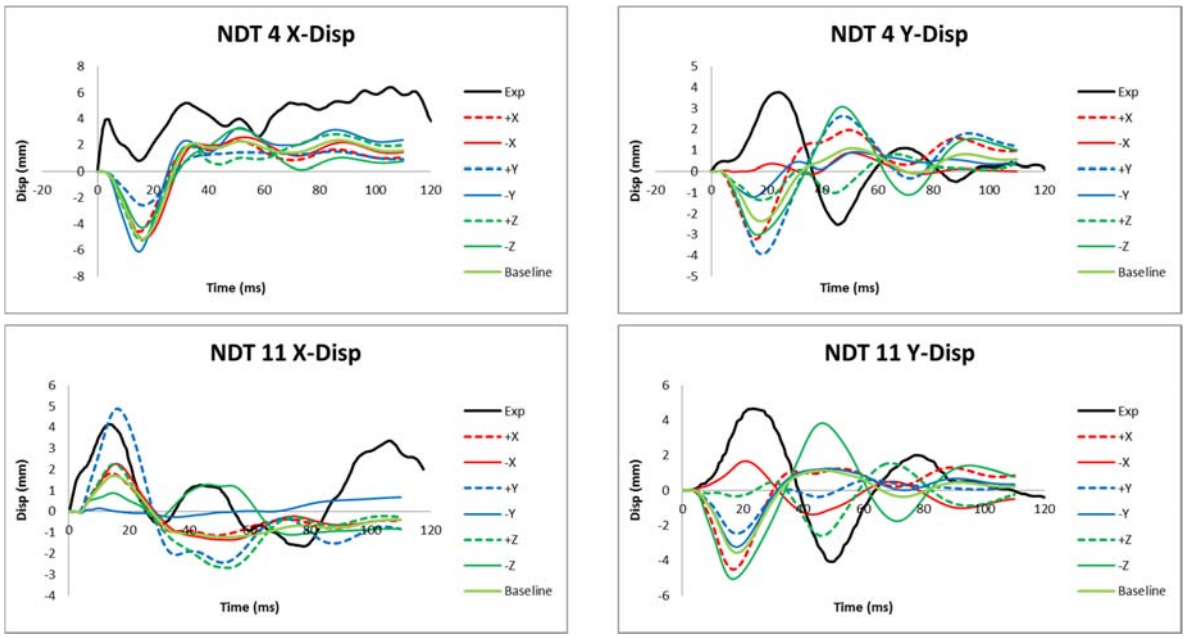

Figs. 45-48: C380-T2 NDT offset NDT location displacement histories.

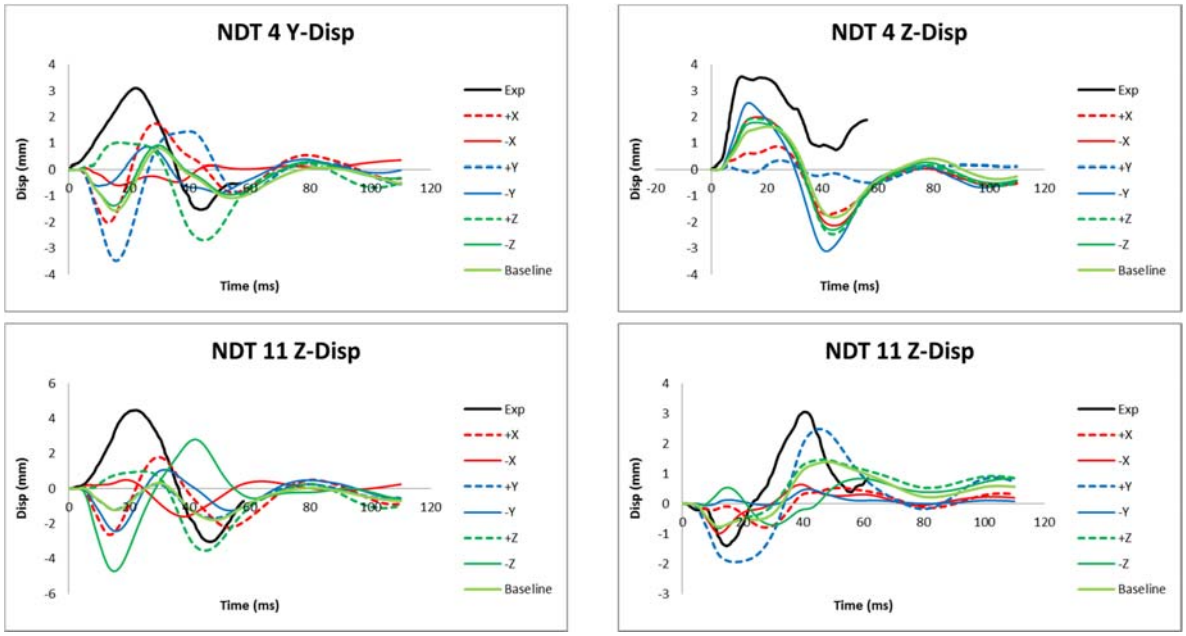

Figs. 49-52: C380-T3 NDT offset NDT location displacement histories.

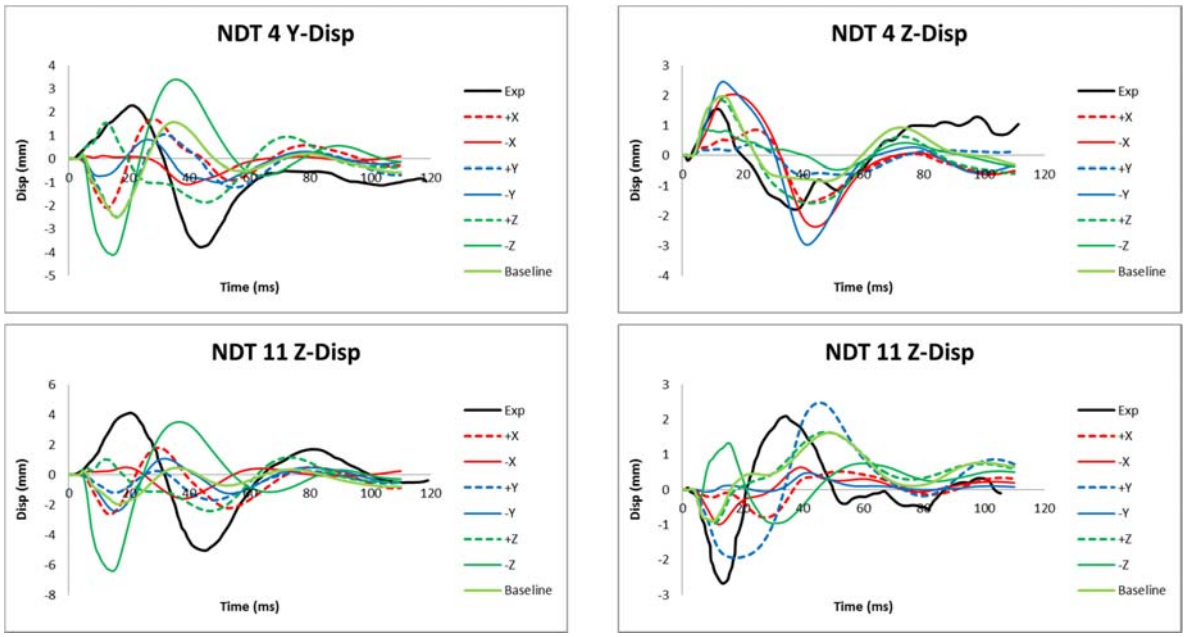

Figs. 53-56: C380-T4 NDT offset NDT location displacement histories.

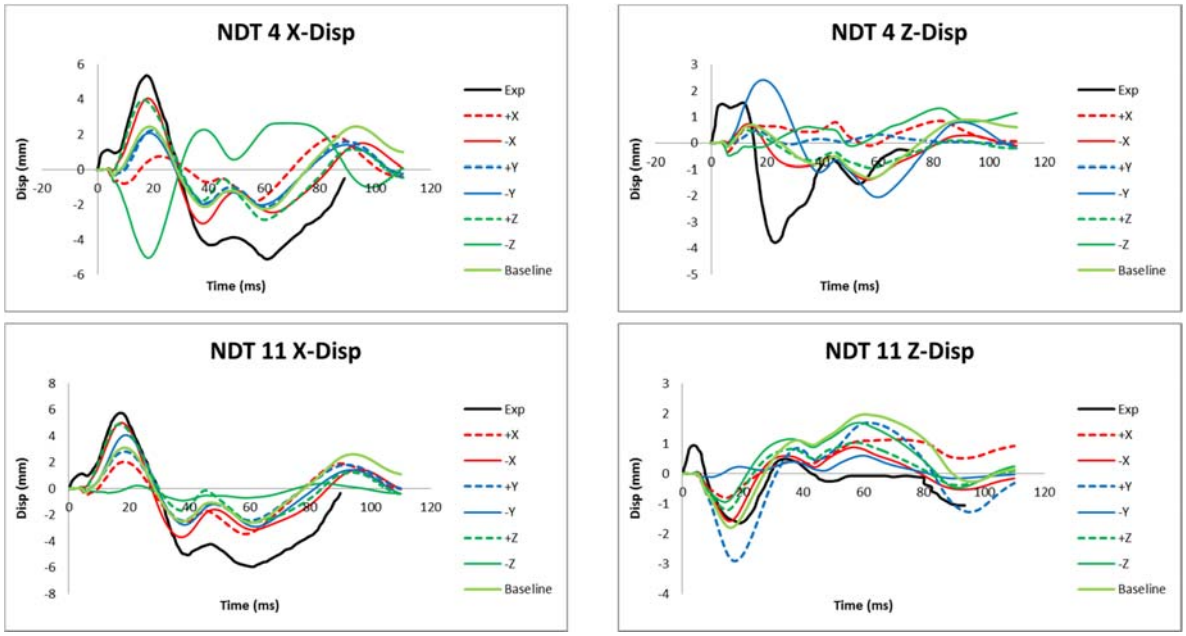

Figs. 57-60: C393-T4 NDT offset NDT location displacement histories.

Appendix B: Numerical Results

NDT Mass

				%Δ NRMSE		
			Baseline	Actual	x5	x10
C288-T3	C1	X	0.69	-0.51%	-3.60%	-7.02%
		Z	1.11	-0.18%	0.93%	2.45%
	C2	X	0.77	-1.69%	-6.44%	-11.76%
		Z	0.84	0.11%	2.17%	4.88%
C380-T2	C1	Y	0.85	-0.36%	-0.10%	0.22%
		X	1.51	-0.36%	-1.19%	-2.22%
	C2	Y	0.95	-0.31%	0.12%	0.65%
		X	1.47	0.04%	-0.56%	-1.30%
C380-T3	C1	Y	1.20	-2.47%	-6.73%	-12.01%
		Z	0.90	3.93%	4.04%	4.21%
	C2	Y	1.01	-1.01%	-3.99%	-7.71%
		Z	0.73	-0.62%	-0.33%	0.03%
C380-T4	C1	Y	1.34	-3.91%	-4.69%	-5.52%
		Z	0.67	-1.66%	-1.46%	-1.09%
	C2	Y	1.15	-6.38%	-7.75%	-9.38%
		Z	0.96	-6.33%	-7.16%	-8.18%
C393-T4	C1	X	0.69	-7.34%	-9.21%	-11.45%
		Z	0.94	-0.32%	-0.80%	-1.37%
	C2	X	0.67	-3.86%	-5.04%	-6.43%
		Z	1.85	5.24%	4.63%	3.90%
	Better Fit			16	15	13
	Worse Fit			4	5	7
	Better Fit (All)				44	
	Worse Fit (All)				16	

Table 1: Percent change in NRMSE due to added NDT Mass. This table gives the impact case, the NDT cluster (C1 or C2), the displacement directions, the baseline NRMSE and the percent change in NRMSE for each NDT mass value added. Green boxes indicate an improved fit with experiment and red boxes indicate a worsened fit. The number of cases that made the fit better or worse is also given at the bottom of the table.

Table 2: Percent change in MPS and CSDM due to added NDT Mass. Green boxes indicate a decrease in strain and red boxed indicate an increase in strain.

Impact Case	Baseline MPS	%Δ MPS		
		Actual	x5	x10
C288-T3	7.80E-01	0.01%	0.06%	0.11%
C380-T2	4.42E-01	0.05%	0.24%	0.48%
C380-T3	3.52E-01	0.04%	0.21%	0.42%
C380-T4	5.82E-01	0.05%	0.23%	0.45%
C393-T4	4.01E-01	0.02%	0.21%	0.50%

Impact Case	Baseline CSDM	%Δ CSDM		
		Actual	x5	x10
C288-T3	2.72E-02	-0.17%	0.69%	0.02%
C380-T2	6.37E-02	-0.10%	-1.11%	-1.26%
C380-T3	1.45E-02	0.26%	-0.58%	-1.91%
C380-T4	1.36E-01	0.20%	-0.03%	0.02%
C393-T4	3.80E-02	-0.09%	1.94%	4.26%

Head Size/Shape Variations

Table 3: Percent change in NRMSE due to model scaling. Positive scaling often worsened the fit with experiment while negative scaling improved the fit.

				%Δ NRMSE							
			Baseline	+X	+Y	+Z	+XYZ	-X	-Y	-Z	-XYZ
C288-T3	C1	X	0.69	-9.58%	8.87%	14.46%	11.44%	28.55%	2.73%	11.66%	22.62%
		Z	1.11	-5.05%	0.34%	12.86%	8.88%	-2.98%	-3.99%	-7.38%	-12.57%
	C2	X	0.77	-11.61%	10.19%	-6.87%	-6.41%	-3.50%	-8.68%	-8.13%	-3.24%
		Z	0.84	6.17%	1.14%	-7.10%	-1.06%	-7.35%	0.48%	4.42%	3.98%
C380-T2	C1	Y	0.85	9.71%	-2.18%	2.02%	9.60%	-1.13%	2.20%	0.47%	0.22%
		X	1.51	2.80%	7.28%	7.18%	23.35%	-7.83%	-11.08%	-9.73%	-22.32%
	C2	Y	0.95	22.34%	-3.11%	9.91%	7.34%	0.98%	21.02%	0.75%	-0.04%
		X	1.47	1.12%	3.00%	12.50%	18.21%	-6.33%	-17.32%	-21.35%	-22.30%
C380-T3	C1	Y	1.20	12.96%	5.67%	6.75%	24.05%	-8.06%	-9.31%	-10.20%	-18.16%
		Z	0.90	-3.85%	-9.79%	9.85%	-8.54%	2.37%	14.38%	2.28%	9.71%
	C2	Y	1.01	0.31%	-10.84%	41.16%	41.29%	-5.68%	3.58%	-5.37%	-3.67%
		Z	0.73	-1.14%	10.74%	21.94%	-5.76%	-5.86%	-2.26%	8.84%	-4.44%
C380-T4	C1	Y	1.34	4.51%	1.68%	2.64%	25.51%	-14.69%	-12.74%	-25.76%	-13.78%
		Z	0.67	6.57%	36.34%	42.54%	19.69%	2.32%	19.24%	4.47%	4.41%
	C2	Y	1.15	-4.10%	-7.22%	30.74%	37.66%	-10.40%	-3.58%	-11.70%	-8.86%
		Z	0.96	-13.28%	9.77%	19.76%	1.36%	3.82%	-2.24%	-6.30%	3.36%
C393-T4	C1	X	0.69	-8.72%	-14.43%	5.97%	-4.30%	-6.04%	0.19%	-5.41%	1.55%
		Z	0.94	1.27%	-14.27%	22.72%	5.48%	-2.99%	12.57%	-7.69%	-4.15%
	C2	X	0.67	-4.31%	-19.56%	-3.45%	-26.71%	-2.49%	16.73%	17.66%	25.99%
		Z	1.85	-12.30%	-14.63%	66.16%	31.88%	-12.01%	-26.42%	-43.92%	-55.16%
		Better Fit		10	9	3	6	15	10	12	12
		Worse Fit		10	11	17	14	5	10	8	8
				Better Fit (+)		28		Better Fit (-)		49	
				Worse Fit (+)		52		Worse Fit (-)		31	

Table 4: Percent change in MPS and CSDM due to model scaling. Positive scaling almost always increased strains while negative scaling decreased strains.

Impact Case	Baseline MPS	%Δ MPS							
		+X	+Y	+Z	+XYZ	-X	-Y	-Z	-XYZ
C288-T3	7.80E-01	13.93%	-6.24%	11.15%	16.63%	-15.98%	7.96%	-9.57%	-19.43%
C380-T2	4.42E-01	13.85%	-0.10%	5.27%	21.71%	-14.90%	-3.23%	-4.85%	-20.02%
C380-T3	3.52E-01	10.80%	9.31%	12.02%	19.34%	-4.87%	2.54%	-6.66%	-13.42%
C380-T4	5.82E-01	14.68%	9.73%	6.86%	14.10%	-12.22%	5.22%	-3.44%	-12.07%
C393-T4	4.01E-01	3.54%	22.08%	21.09%	25.24%	-2.10%	-1.32%	-5.59%	-16.32%

Impact Case	Baseline CSDM	%Δ CSDM							
		+X	+Y	+Z	+XYZ	-X	-Y	-Z	-XYZ
C288-T3	2.72E-02	80.72%	-6.91%	48.87%	112.90%	-36.50%	17.13%	-25.69%	-56.35%
C380-T2	6.37E-02	93.61%	9.44%	34.63%	144.88%	-63.99%	-3.21%	-26.30%	-78.12%
C380-T3	1.45E-02	112.29%	48.39%	134.19%	281.64%	-48.22%	5.55%	-34.96%	-84.36%
C380-T4	1.36E-01	22.09%	21.17%	10.62%	59.58%	-22.18%	-12.48%	-3.94%	-39.75%
C393-T4	3.80E-02	39.63%	52.46%	114.89%	201.96%	-23.66%	-22.60%	-50.12%	-84.59%

NDT Location Variations

Table 5: Percent change in NRMSE due to NDT location offsets. Negative X and positive Z NDT location shifts almost always improved the fit with experiment.

				%Δ NRMSE					
			Baseline	+X	-X	+Y	-Y	+Z	-Z
C288-T3	C1	X	0.69	26.05%	-0.04%	34.02%	11.70%	-20.92%	82.73%
		Z	1.11	-2.48%	-13.53%	-10.47%	-0.47%	-2.74%	-12.32%
	C2	X	0.77	-2.09%	-1.52%	19.10%	-8.25%	-27.99%	56.45%
		Z	0.84	17.63%	-5.15%	7.60%	0.40%	-2.24%	-0.13%
C380-T2	C1	Y	0.85	2.45%	3.00%	-0.72%	-6.40%	-0.57%	10.01%
		X	1.51	11.65%	-31.19%	33.73%	-21.66%	-24.63%	28.75%
	C2	Y	0.95	-1.25%	-0.26%	19.15%	-3.68%	16.90%	5.26%
		X	1.47	4.25%	-45.80%	-15.81%	-2.90%	-40.91%	31.91%
C380-T3	C1	Y	1.20	-1.72%	-4.15%	49.59%	-26.24%	-15.25%	-5.07%
		Z	0.90	15.06%	3.78%	11.19%	20.38%	8.03%	8.38%
	C2	Y	1.01	7.64%	-7.31%	-0.16%	18.97%	-30.66%	76.61%
		Z	0.73	37.34%	8.04%	24.14%	23.62%	-11.37%	59.06%
C380-T4	C1	Y	1.34	-16.98%	-38.83%	-11.71%	-38.18%	-42.19%	38.90%
		Z	0.67	50.96%	77.45%	24.70%	73.02%	12.16%	36.21%
	C2	Y	1.15	-7.70%	-26.26%	-20.36%	-1.57%	-34.64%	58.85%
		Z	0.96	15.08%	-17.48%	30.06%	1.49%	-0.61%	54.99%
C393-T4	C1	X	0.69	36.10%	-26.44%	4.75%	2.59%	-19.67%	136.52%
		Z	0.94	29.08%	-17.66%	11.70%	45.26%	-6.97%	27.96%
	C2	X	0.67	-3.40%	-31.29%	1.72%	-12.13%	-6.78%	38.96%
		Z	1.85	-23.88%	-56.50%	-18.86%	-39.24%	-41.50%	-11.92%
	Better Fit			8	16	7	11	17	4
	Worse Fit			12	4	13	9	3	16

Peak-To-Peak Displacements (all cases)

Table 6: Changes in Peak-To-Peak NDT displacements for all model variations. Experimental and baseline P2P displacements and the percent difference between the two are given as well. Percent change from baseline cells are color formatted: blue indicates decreases in P2P displacement and red indicates increases with more intensely colored cells indicating larger changes.

			Exp.	Baseline	% Δ	NDT Masses			Scaling								Offsets					
						Actual	x5	x10	+X	+Y	+Z	+XYZ	-X	-Y	-Z	-XYZ	+X	+Y	+Z	-X	-Y	-Z
C288-T3	NDT 4	X	5.97	2.30	-61.5%	1.7%	8.8%	18.0%	17.0%	-22.9%	-22.4%	-11.3%	-44.3%	15.3%	-15.6%	-22.9%	-42.0%	-60.6%	62.2%	1.4%	29.6%	17.3%
		Z	3.92	2.18	-44.3%	0.6%	3.4%	6.9%	-19.5%	-9.9%	38.8%	13.4%	5.9%	1.4%	-26.1%	-29.4%	12.8%	-55.8%	-12.9%	-56.1%	14.8%	-20.7%
	NDT 11	X	4.13	1.37	-66.9%	4.8%	23.8%	47.4%	36.8%	-10.9%	10.0%	33.7%	5.2%	73.2%	19.2%	56.3%	17.8%	-47.5%	182.1%	2.2%	109.9%	90.7%
		Z	4.56	1.77	-61.2%	-0.1%	-0.6%	-0.7%	-10.5%	-1.4%	35.2%	7.1%	37.8%	12.2%	-29.5%	-6.8%	-61.1%	-70.3%	-0.1%	78.8%	15.3%	-15.5%
C380-T2	NDT 4	Y	6.38	7.50	17.5%	0.2%	1.0%	2.0%	35.3%	-14.8%	14.4%	30.4%	-23.3%	13.6%	-4.9%	-10.1%	-8.1%	-45.9%	7.6%	2.8%	25.5%	0.0%
		X	6.29	3.46	-45.0%	-0.6%	-2.8%	-5.5%	9.2%	19.7%	22.5%	67.1%	-14.4%	-23.2%	-18.2%	-32.3%	49.9%	89.8%	-37.8%	-71.3%	-38.3%	76.0%
	NDT 11	Y	5.80	2.92	-49.7%	-0.1%	-0.2%	-0.3%	72.7%	-36.0%	26.8%	38.4%	-18.5%	88.1%	2.1%	15.8%	1.5%	150.9%	69.0%	24.0%	-67.6%	-17.9%
		X	8.71	4.70	-46.1%	-0.5%	-2.0%	-3.7%	0.2%	12.1%	26.4%	44.7%	-13.5%	-41.3%	-41.8%	-41.9%	23.7%	-34.9%	-11.8%	-35.0%	-4.7%	89.3%
C380-T3	NDT 4	Y	4.61	2.35	-49.1%	3.8%	-2.8%	-8.6%	10.7%	12.0%	-12.5%	6.1%	6.9%	-26.0%	4.3%	-17.7%	60.5%	109.3%	57.6%	-59.9%	-25.9%	-2.6%
		Z	3.51	3.43	-2.3%	0.0%	2.3%	5.2%	7.4%	-38.1%	67.9%	25.0%	-6.2%	41.0%	-39.2%	-6.7%	-24.8%	-75.7%	28.1%	20.1%	64.0%	18.8%
	NDT 11	Y	7.51	2.11	-71.9%	3.1%	5.8%	9.2%	-2.6%	30.9%	70.9%	68.0%	28.2%	-17.1%	6.0%	-7.8%	109.7%	-7.6%	114.3%	-0.6%	66.0%	256.5%
		Z	4.45	2.16	-51.5%	-1.5%	-1.6%	-1.6%	-5.0%	-53.3%	46.8%	-14.9%	-17.5%	30.7%	-43.3%	-17.7%	-39.1%	104.8%	5.0%	-24.5%	-74.9%	-28.1%
C380-T4	NDT 4	Y	6.06	4.08	-32.7%	-7.3%	-10.2%	-13.7%	-6.8%	13.8%	-4.1%	32.9%	-14.7%	-33.3%	-16.1%	-42.0%	-7.2%	-13.9%	-16.8%	-70.3%	-55.4%	84.3%
		Z	3.34	2.82	-15.4%	4.3%	6.4%	9.0%	20.8%	-59.8%	81.4%	-18.7%	-6.5%	59.1%	-34.1%	-15.0%	-14.2%	-64.4%	22.2%	56.2%	92.2%	-52.5%
	NDT 11	Y	9.15	2.42	-73.5%	2.3%	-4.2%	-12.3%	-8.0%	12.6%	162.7%	169.3%	15.0%	8.2%	-4.2%	-1.6%	82.5%	-19.6%	47.4%	-13.5%	44.5%	309.6%
		Z	4.77	2.53	-47.0%	1.2%	2.0%	3.1%	-8.0%	-41.8%	43.3%	-1.0%	-12.4%	44.4%	-38.1%	-18.7%	-47.9%	75.1%	3.6%	-35.5%	-78.5%	-9.2%
C393-T4	NDT 4	X	10.49	4.70	-55.2%	2.4%	6.6%	12.0%	8.8%	22.7%	-22.8%	3.3%	-0.9%	-15.4%	8.0%	-8.6%	-22.0%	-7.9%	45.2%	51.7%	-13.1%	63.2%
		Z	5.32	2.21	-58.5%	-5.2%	-4.0%	-2.5%	-15.2%	-26.3%	38.5%	5.8%	6.0%	7.7%	-43.7%	-25.0%	-46.9%	-76.7%	-35.4%	-4.9%	101.7%	-17.8%
	NDT 11	X	11.70	5.71	-51.2%	0.7%	3.8%	7.7%	7.6%	29.8%	-13.8%	30.9%	-3.3%	-15.9%	122.5%	-36.4%	-3.8%	-7.9%	30.8%	52.4%	22.2%	-77.2%
		Z	2.59	3.77	45.8%	0.8%	2.0%	3.6%	6.0%	-29.8%	62.4%	22.9%	-9.4%	15.3%	-39.9%	-33.3%	-48.7%	21.8%	-40.4%	-35.0%	-79.9%	-30.0%
						Actual	x5	x10	+X	+Y	+Z	+XYZ	-X	-Y	-Z	-XYZ	+X	+Y	+Z	-X	-Y	-Z
		Raw Average			-41.0%	0.5%	1.9%	3.8%	7.8%	-9.6%	33.6%	27.6%	-4.0%	11.9%	-11.6%	-15.1%	-0.4%	-1.8%	26.0%	-5.8%	7.4%	36.7%
		Average Magnitude			47.3%	2.1%	4.7%	8.7%	15.4%	24.9%	41.2%	32.2%	14.5%	29.1%	27.8%	22.3%	36.2%	57.0%	41.5%	34.8%	51.2%	63.9%